Structure of Growing Microtubule Ends: Two-Dimensional Sheets Close Into Tubes at Variable Rates

Denis Chrétien, Stephen David Fuller, and Eric Karsenti

European Molecular Biology Laboratory, D-69117 Heidelberg, Germany

Abstract. Observation of microtubule growth at different rates by cryo-electron microscopy reveals that the ends range from blunt to long, gently curved sheets. The mean sheet length increases with the growth rate while the width of the distributions increases with the extent of assembly. The combination of a concentration dependent growth rate of the tubulin sheet with a variable closure rate of the microtubule cylinder, results in a model in which stochastic fluctuations in sheet length and tubulin conformation confine GTP-tubulins to microtubule ends. We propose that the variability of microtubule growth rate observed by video microscopy (Gildersleeve, R. F., A. R. Cross, K. E. Cullen, A. P. Fagen, and R. C. Williams. 1992. *J. Biol. Chem.* 267: 7995–8006, and this study) is due to the variation in the rate of cylinder closure. The curvature of the sheets at the end of growing microtubules and the small oligomeric structures observed at the end of disassembling microtubules, indicate that tubulin molecules undergo conformational changes both during assembly and disassembly.

MICROTUBULES are polymers of the tubulin molecule forming polar hollow cylinders. In most cells, these structures are either stabilized by interactions with other components or exist in a dynamic state, exchanging subunits with a pool of free tubulin dimers through the mechanism of dynamic instability. This behavior is an intrinsic property of microtubules assembled from pure tubulin (Mitchison and Kirschner, 1984*a*,*b*). At low free tubulin concentration, microtubules are either growing slowly or shrinking rapidly, the interconversion between these two phases being infrequent (Horio and Hotani, 1986). The frequency of conversion from growing to shrinking (catastrophe) decreases with increasing tubulin concentration while the frequency of the complementary event (rescue) increases (Walker et al., 1988, 1991). Dynamic instability has also been observed in vivo and is particularly clear during mitosis. This unusual dynamic behavior provides the plasticity to the microtubule network which enables the reorganization of microtubules during the cell cycle and cell differentiation (for reviews see Bayley et al., 1994; Kirschner and Mitchison, 1986; Wordeman and Mitchison, 1994).

The decrease of catastrophe frequency with increasing tubulin concentration has motivated the assumption that microtubules are stabilized by a specific structure at their ends. In their original study, Mitchison and Kirschner (1984*a*,*b*) proposed that microtubule ends were stabilized by a layer of GTP-liganded tubulin molecules which capped the unstable guanosine 5′-diphosphate (GDP)[1]–microtubule lattice. At low growth rate the cap was supposed to be sufficiently short to allow catastrophes. Cap size was supposed to increase with growth rate to explain the absence of catastrophes at the highest tubulin concentrations. The determination of the size of this GTP–cap and its correlation with the microtubule growth rate has been very difficult (for reviews see Caplow, 1992; Erickson and O'Brien, 1992). A recent investigation by Drechsel and Kirschner (1994) has established that only a few GTP containing subunits at the tip of the microtubule are sufficient to stabilize a growing microtubule. Their study suggests that GTP hydrolysis closely follows the addition of the tubulin subunits to the end of the microtubule. Catastrophic depolymerization would begin when one of the GTP subunits is converted to GDP with a corresponding weakening of lateral interactions. It remains unclear whether loss of GTP subunits is entirely stochastic or regulated by a structural change accompanying microtubule assembly.

Recent electron microscope studies have unambiguously shown that the ends of growing and shrinking microtubules have different conformations (Simon and Salmon, 1990; Mandelkow et al., 1991), however the relationship between microtubule end structure and growth rate has not yet been established. In this work, we have examined whether the differential stability of slowly and rapidly growing microtubules could be correlated with differences

Address all correspondence to D. Chrétien, European Molecular Biology Laboratory, Meyerhofstrasse 1, D-69117 Heidelberg, Germany. Tel.: (49) 6221 387298. Fax: (49) 6221 387306.

1. *Abbreviations used in this paper*: DIC, differential interference contrast; GDP, guanosine 5′-diphosphate.

in the structure of their ends. We find outwardly curved sheets of variable length at the end of growing microtubules. The average length of these sheets increases with microtubule growth rate. We propose a simple model of microtubule elongation based on the uniform growth of a tubulin sheet and its subsequent closure at a variable rate into the microtubule cylinder. In this model, GTP–hydrolysis would be induced by or be concomitant with a conformational change of the tubulin dimer occuring before cylindrical closure. This conformational change could also be "forced" when cylindrical closure moves rapidly towards the extremity of the growing sheet. This behavior could regulate the transition frequency between growth and shrinkage.

Materials and Methods

Preparation of Pure Tubulin from Bovine Brain

Tubulin was isolated from calf brain by two cycles of assembly–disassembly in the presence of glycerol, followed by phosphocellulose chromatography and was obtained in 50 mM Pipes, 1 mM EGTA, 0.2 mM $MgCl_2$, pH 6.8 with KOH (Maaloum et al., 1994). The peak flow through fractions coming from the phosphocellulose column were adjusted to 1 mM GTP, aliquoted, snap frozen, and stored in liquid nitrogen. SDS gel electrophoresis was carried out on 7.5% polyacrylamide gels (Protean II mini cuves; Bio-Rad Laboratories GmbH, München, Germany) stained with Coomassie brilliant blue. No detectable traces of contaminating MAPs could be found.

Determination of the Tubulin Concentration

Tubulin concentration was determined by two methods. We have used the Bradford assay (Bradford, 1976) using the protein assay from Bio-Rad (Bio-Rad protein assay) and bovine serum albumin (A 9649; Sigma Chemical Co., St. Louis, MO) as a standard for routine determination of protein concentration. Optical readings were done after 15 min of color development. Because the Bradford assay can give widely different color developments with different proteins, we adopted a more rigorous method to standardize the tubulin concentration. An amino acid analysis of a 1-μl aliquot of the sample used in our experiments was performed by the Biochemical Instrumentation group at the EMBL (Heidelberg, Germany). The total number of amino acids of each type was determined in the sample and their proportions were compared to the expected number of amino acids known from the sequence (because we could not find any report on the sequence of calf brain tubulin, we choose the pig brain tubulin sequence as a reference (Krauhs et al., 1981; Ponstingl et al., 1981). The total tubulin concentration was found to be 4.8 μg by amino acid analysis compared to the expected value of 7.4 μg as estimated by the Bradford assay. Hence, the concentration of tubulin is overestimated by 1.6-fold when determined by the Bradford assay using bovine serum albumin as a standard. Values given in this paper are based on the tubulin concentration as determined by the amino acid analysis.

Isolation of Centrosomes from KE-37 Cells

Centrosomes were isolated from KE-37 human lymphoid cells by a slight modification of the protocol described by Bornens et al. (1987) to give centrosome concentrations suitable for cryo-electron microscopy (~4.10^8/ml) and video microscopy (~1.10^8/ml), (the detailed protocol will be reported elsewhere). The centrosome concentration was determined by electron microscopy after sedimentation of a known volume on a carbon coated grid. Centrosome concentrations given in this paper are expressed in terms of pairs of centrioles, i.e., the total concentration of single centrioles divided by two. The fraction of paired centrioles was ~40% in our preparations.

Sample Preparation for Video Microscopy

We used video-enhanced differential interference contrast (DIC) light microscopy to follow microtubule dynamics (Allen, 1985; Salmon et al., 1989). Tubulin was thawed and centrifuged in an Eppendorf centrifuge at 14,000 rpm, 15 min, 4°C. The centrosome and tubulin solutions were adjusted to 80 mM Pipes, 1 mM EGTA, 1 mM $MgCl_2$, pH 6.9, and 1 mM GTP, before assembly. One volume of centrosomes (1.10^8/ml) was mixed with three volumes of tubulin at varying concentrations (see Results). The preparation of centrosomes and tubulin at the desired concentration was introduced into home-made chambers with a volume of about 20 μl (10-mm diam and ~260-μm deep; fabricated by the Mechanical Workshop at the EMBL). We found that the activity of tubulin decreased upon injection into the glass chamber. This artifact was first detected by studying microtubule polymerization close to the critical concentration for assembly by both video microscopy and cryo-electron microscopy. Microtubules could be observed by electron microscopy while none were observed by video microscopy for an identical tubulin concentration. This observation suggested that depletion of tubulin occurred by adsorption to the glass coverslips. To restore tubulin activity, it was necessary to flow a large volume (100 to 200 μl depending on tubulin concentration) of pure tubulin into the chamber. The slide was then placed on the stage of a Zeiss Axiovert 10 photo microscope (Carl Zeiss Ltd, Oberkochen, Germany). Stage, condenser and objective lens were heated to 37°C using a home-made apparatus designed by the Electronic and Mechanical Workshops at the EMBL. The temperature of the specimen could be accurately checked by introducing a small thermocouple (0.25-mm diam; Thermocoax, Philips GmbH, Hamburg, Germany) inside the cell. Temperature gradient in the vertical direction was eliminated by adjusting the temperature in the oil above and below the coverslips to 37°C.

Video-enhanced Differential Interference Contrast Light Microscopy

After injection of the pure tubulin solution into the chamber pre-coated with centrosomes, the slide was placed on the stage of the microscope and the timer was started when both the objective and condenser were in contact with the oil on the coverslips. The microscope was equipped with DIC prisms, a Zeiss Achrostigmat 100×/1.25 NA oil immersion objective lens, and an intermediate 1.6× magnification lens. We used an HBO 50 W mercury lamp coupled to an optical scrambler (Technical Video, Ltd., Woods Hole, MA) to obtain homogeneous illumination at the CCD video camera faceplate (C 3077; Hamamatsu Photonics K. K., Sunayamo-Cho, Japan). Light was transmitted through heat-cut and 546 nm interference filters. The field of view was 33-μm wide corresponding to a pixel size of 64 nm (horizontal direction) at the object. Images were electronically enhanced (C 2400; Hamamatsu) and were transferred to a laser videodisc (laser videodisc media LVM-3AAO; Sony) via an Argus 10 image processor (Hamamatsu). The Image processor and the laser videodisc were controlled using a program written by S. Albrecht and E. Stelzer (Physical Instrumentation Programme, EMBL). Images were recorded at 1-s interval for typical periods of 5 min. Several sequences were recorded for each condition.

Analysis of Microtubule Dynamics

Microtubule dynamics were analyzed using NIH-Image 1.48 (National Institutes of Health, Bethesda, MD) on a Macintosh IIci or a Macintosh Quadra 800 (Apple Computer, Inc., Cupertino, CA). A cross was overlaid on the image at the beginning of a microtubule near the centrosome and remained at this position throughout the analysis. Microtubule length measurements were performed using the line tool provided in NIH Image. The line was started at the cross defining the beginning of the microtubule and ended at its extremity. Only extremities giving a sharp image were measured. When microtubules were curved, the length was approximated by a segmented line. The length-time-frame data were transferred to KaleidagraphTM 2.1 (Synergy Software, PCS Inc., Reading, PA) and analyzed as follows (see Fig. 1 *b*). A scatter plot of the length versus time was obtained and smoothed using the weighted curve fit provided in KaleidagraphTM (see Chambers et al., 1983). This curve fitting method is quite insensitive to outliers and follows the long range variations of the rates. The smoothing factor was adjusted by eye until the curve passed evenly through the points (no correlation coefficient is defined by this algorithm). We used two programs to determine the dynamical parameters. The first program determined the rates along the fitted curve at time intervals corresponding to the length measurements and discriminated growth phases from shrinking phases by means of a rate threshold (close to 0.0 μm/min or slightly negative). The program then calculates the time spent in the corresponding phases and the resulting frequency of catastro-

phe and rescue. The second program was used when the length versus time plot showed elongation followed by rapid shortening so that the weighted curve fit could not be used to accurately determine the rates. Growing and shrinking phases were then fitted separately and rates were determined as in the first method. This procedure gives a reasonable approximation of the long range variations of the rates and does not change the number of experimental points which allows the comparison of different conditions using the χ^2 statistic. However, they do this at the expense of maintaining the same weight for all rate measurements independently of the duration between two length measurements.

Preparation of Holey-carbon Coated Grids for Cryo-electron Microscopy

We adapted the protocol of Fumaki and Adachi (1965) to obtain holey-carbon coated grids of suitable hole sizes to observe microtubule assembly from centrosomes. The protocol described below is also more rapid and avoids the use of an hydrating agent to remove the plastic film from the glass slide.

Histological glass slides, pre-cleaned in ethanol, were plunged in a solution of 0.1% Tween 20, removed vertically taking care to avoid the formation of bubbles and air dried vertically on a filter paper. The detergent-treated slide was deposited at the surface of an aluminium bloc pre-cooled at −15°C and let stand flat for 15 to 30 s (the ambient humidity was about 65%). When condensation was covering its surface, the slide was removed and a solution of pre-filtered 0.25% cellulose acetate butyrate (Aldrich Chemie, Steinheim, Germany) in ethyl acetate was overlaid homogeneously on its surface and the excess of solution was immediately discarded. Slides were air dried vertically and the holes were examined with a phase microscope. The holey-plastic film was freed from the slide by plunging it obliquely into distilled water. Pre-cleaned copper, electron microscope grids (mesh size between 100 and 400) were deposited on the plastic film and the preparation was recovered with a piece of newspaper overlaid on its surface. The preparation was air dried and heavily coated with carbon. Grids were deposited at the surface of a filter paper impregnated with chloroform to remove the plastic. Finally, the grids were carefully selected for their hole sizes depending on the experiments to be carried out. Grids with smaller holes (~5 μm) were used to observe isolated centrosomes and microtubules at short assembly times and ones with larger holes (~10 μm) were used to observe longer times of assembly.

Preparation of Vitrified Samples for Cryo-electron Microscopy

Vitrified specimens were prepared according to Dubochet et al. (1985) using the environmental device described by Chrétien et al. (1992). This device allows the control of temperature and humidity around the specimen when it stand on the electron microscope grid before vitrification. Specimen preparation was identical as for video microscopy except that the more concentrated centrosome fractions were used (~4.0×10^8/ml). Microtubule assembly was performed directly on the grid. A 4-μl droplet of the suspension kept on ice was deposited on the electron microscope grid standing vertically over a small cup of liquid ethane. The droplet was warmed to 37°C by the humid air from the environmental device. The temperature of the specimen could be precisely controlled using a fine thermocouple (0.25-mm diam; Thermocoax) placed within the droplet itself. After assembly for various times at 37°C (see Results) the grid was blotted with a filter paper and quickly plunged into liquid ethane. To study depolymerization, microtubules were assembled as before, and then the droplet was partially blotted with a filter paper applied to the edge of the grid so that ~1 μl remained and a volume of 10 μl of pre-warmed buffer was immediately added. After about 30 s the grid was blotted and plunged into liquid ethane. Specimen grids were stored in liquid nitrogen until observation.

The specimen grids were transferred to a Gatan stage (Gatan GmbH, München, Germany) pre-cooled with liquid nitrogen and were observed with a 400 Philips electron microscope (Philips Electronics Instruments, Eindhoven, Netherlands) operating at 80 kV. Centrosomes and microtubules were located at low magnification (2,300×) under low electron dose conditions. One image was taken at a magnification of 14,800× or 19,800× and ~1.5-μm underfocus and a second image was taken at 8,200× or 10,900× and ~8 μm underfocus. Occasionally tilted views were taken with tilt angles ranging from 3° to 10°. Negatives (SO-163; Eastman Kodak Co., Rochester, NY) were developed in full-strength developer (D19; Eastman Kodak Co.) for 10 min.

Measurement of Microtubule End Extension Lengths

Negatives were digitized using a CCD camera (XC-77CE; Sony Co., Japan) and images were acquired using NIH Image 1.48 on a Macintosh IIcx. Extensions were measured using the line tool provided in NIH Image. A precise definition of the location of the beginning of the extension would require a complete three-dimensional reconstruction for each microtubule, a goal which is far beyond the scope of this study. Hence, we used the contrast present in the microtubule images and the curvature of the extensions as landmarks. Complete microtubules observed by cryo-electron microscopy give characteristic images whose contrast can be interpreted in terms of the number of protofilaments present in the structure (Chrétien and Wade, 1991; Ray et al., 1993; Wade et al., 1990). Apart from the fine variations of contrast due to the skew of protofilaments or changes in protofilament numbers in individual microtubules (Chrétien et al., 1992), the overall contrast and the width of the microtubule image remain constant as long as the microtubule wall is intact. Therefore we defined the end of the microtubule cylinder, and hence the beginning of the extension, as the point where the typical microtubule image was interrupted. This was particularly clear when one of the two edge bands disappeared indicating that the structure was no longer tubular. This definition was assisted by the fact that the extensions curve slightly and hence differ from the straight appearance of the complete microtubule cylinder (see Fig. 6).

Computer Modeling of Microtubule Elongation

Computer simulations were carried out on a DEC 7000-AXP computer. Programs were written in VMS Fortran 4.8 and incorporated subroutines from Numerical Recipes (Press et al., 1992) for the probability distributions of the growth rates and the statistical analysis of the data (the programs are available upon request). Simulations were usually carried out using 10,000 microtubules. The mean values of separate simulations did not vary significantly as long as more than 500 microtubules were followed. Each microtubule was represented by a pair of values (see Fig. 9, *a* and *b*) corresponding to L_c, the length of the cylindrical part of the microtubule and L_{c+s}, the length of the cylindrical part plus the sheet extension. The rate of growth of the sheet, $V_g(s)$, and that of the microtubule cylinder, $V_g(c)$, were set equal. The time step was determined by the length of the subunit (8 nm) divided by the rate. At each step L_{c+s} was incremented by a length corresponding to the sheet rate divided by the time step. The same operation was carried out for L_c except that a value taken at random from a Gaussian distribution of standard deviation $SD_g(c)$ was added to the microtubule cylinder rate. When L_c was greater than L_{c+s}, the program set L_c at the same value as L_{c+s}. The sheet length L_s was calculated by subtracting L_c from L_{c+s}. The microtubule cylinder and sheet lengths were binned at 24-nm intervals at the end of the simulation and the minimum, maximum, mean, standard deviation, variance, skew, and kurtosis of each distribution were determined.

Results

Dynamics of Centrosome-nucleated Microtubules

In order to examine the structure of MTs undergoing dynamic instability by cryo-electron microscopy, we first had to establish proper conditions of dynamic instability by video-microscopy enhanced DIC microscopy. Careful observation of DIC video microscope sequences indicates that microtubules at 37°C and 13 μM tubulin concentration do not elongate at a constant rate (Fig. 1). This confirms the observations of Gildersleeve et al. (1992). Further, microtubules nucleated by the same centrosome can elongate with different rates (Fig. 1 *a*). The uncertainty in determining the precise location of the microtubule extremity necessitates the use of smoothed data to characterize growth rates and their variation. We used a locally weighted least square error fitting method (see Materials and Methods; Chambers et al., 1983; and Fig. 1 *b*).

We then fixed conditions where the microtubules were either growing slowly and showed catastrophes, or were

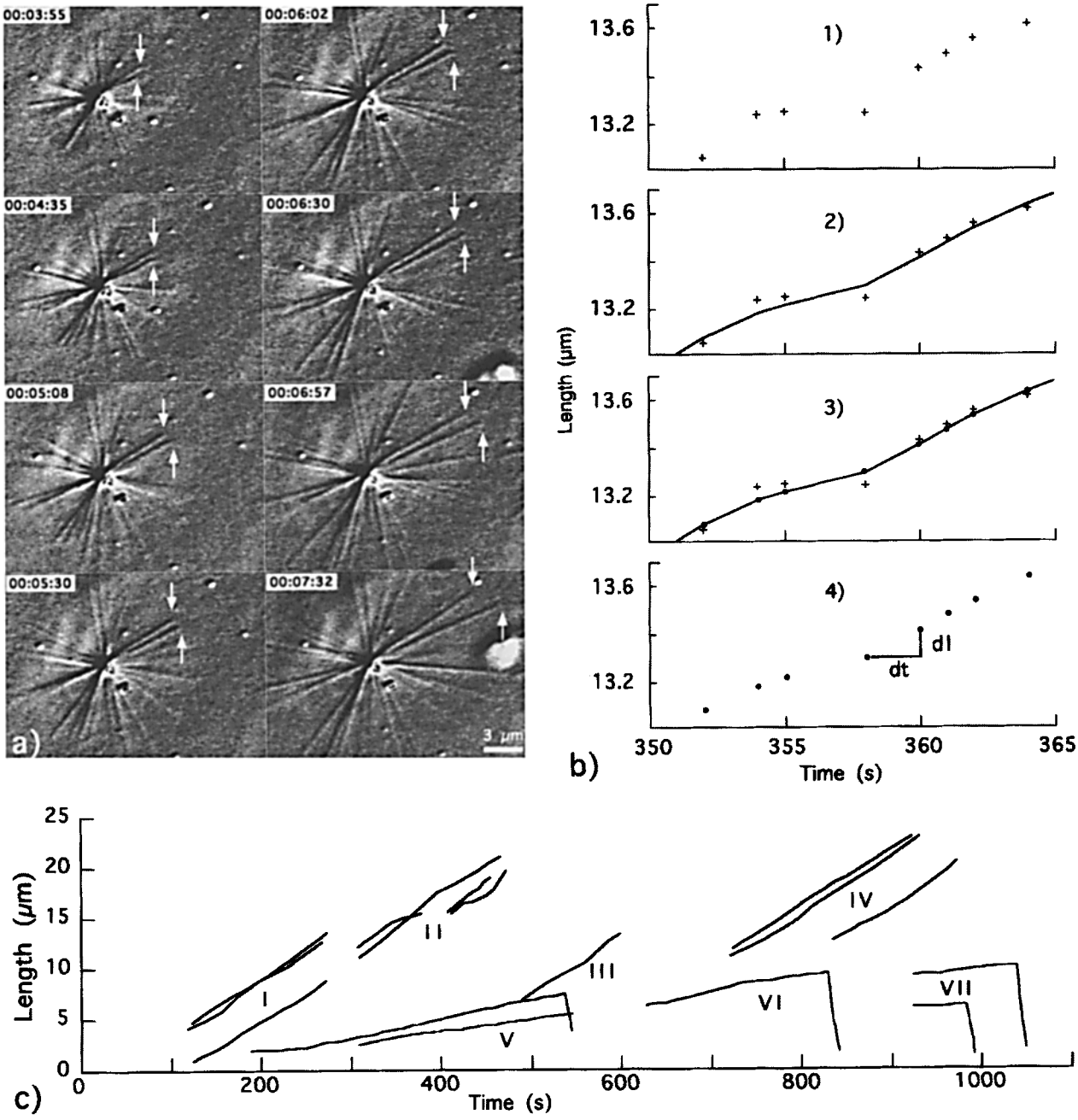

Figure 1. (*a*) Video microscope sequence of a microtubule aster growing in a 13 μM tubulin solution. The timer was started at the beginning of the incubation at 37°C. The time interval between each image is approximately 30 s and the average growth rate of microtubules is about 2 μm/min. The *arrows* mark the extremities of two adjacent microtubules growing at different rates. Note the slightly curved extremity of the bottom microtubule (*arrow*) in the top right panel. (*b*) Determination of the rates. A 15-s sequence of a L(t) plot has been enlarged to demonstrate the method used to determine the rates for a single sequence. A scatter plot of the length versus time measurements is obtained (*1*) and is fitted using a weighted curve fit to reduce experimental errors in measurements (*2*). Corrected length values (*dark circles*) are obtained along the fitted curve at the same time points as the experimental ones (*3*) and rates are determined between each pair of values (*4*). (*c*) Concentration dependence of the catastrophe frequency. Smoothed curves of microtubule length versus time are shown at two different tubulin concentrations. The numbers indicate seven centrosomes for which microtubules were analyzed. Centrosome *I*, 3 microtubules; *II*, 4; *III*, 1; *IV*, 3; *V*, 2; *VI*, 1; *VII*, 2. Centrosomes *I–IV* (*upper traces*), assembly in a 19.5 μM tubulin solution. *Centrosomes V–VII* (*lower traces*) assembly in a 6.5 μM tubulin solution. Catastrophes are only observed at the lowest tubulin concentration (see Table II). Variability of the rates between microtubules under a single condition and for the same microtubule is evident.

continuously growing. Fig. 1 *c* presents the traces of L(t) plots after curve fitting for individual microtubules derived from the analysis of sequences similar to those illustrated in Fig. 1 *a*. We analyzed microtubule dynamics at seven tubulin concentrations in a concentration range where self-assembly did not occur (from 3.2 to 19.5 μM). The average growth rate of microtubules increased linearly with the tubulin concentration (Fig. 2 *a*, linearity test,

Table I. Rate Constants for Centrosome Nucleated Microtubule Assembly and Disassembly

Parameters	Values
Slope ($\mu m/\mu M^{-1}/min^{-1}$)	0.21 ± 0.05
k^+ ($\mu M^{-1}/s^{-1}$)	5.7 ± 1.4
y-intercept ($\mu m/min^{-1}$)	−0.52 ± 0.10
$k^-(s^{-1})$	14.1 ± 2.7
x-intercept (μM)	2.51 ± 0.05
V_s ($\mu m/min^{-1}$)	31.5 ± 6.8
k_s^- (s^{-1})	853 ± 184

Rate constants for assembly were calculated from the growth rate versus tubulin concentration plot in Fig. 2 *a* assuming 1,625 dimers of 8-nm length/μm of microtubule and 13 protofilaments. The dissociation constant k_s^- during rapid disassembly was obtained from the average depolymerization rate of microtubules V_s. All values are given ± the standard deviation of the mean.

$P < 0.05$) as previously reported (Mitchison and Kirschner, 1984*b*; Walker et al., 1988). The rate constants deduced from this analysis are given in Table I. Catastrophes were observed at 4.5 and 6.5 μM and microtubules reached apparent steady state lengths whose theoretical values are given in Table II. Under these conditions, less than 4% of the microtubules were in the shrinking phase. No assembly could be detected either by video or cryo-electron microscopy at 3.2 μM. Above 9.7 μM, no catastrophes were observed and microtubules grew until they disappeared from the field of view. The rates were variable at all tubulin concentrations and their distributions appeared to be Gaussian both for the growing (Fig. 2 *b*) and shrinking phases (Fig. 2 *c*). The rate variations (bars in Fig. 2 *a*) increased with tubulin concentration although the coefficient of variation, expressed as the ratio of the standard deviation to the mean remained approximately constant and equal to 0.4 (see Table III).

Most of these results confirm previous work, but it was essential to establish the dynamic properties of microtubules under our conditions as a preliminary to the structural analysis.

Cryo-electron Microscopy of Centrosome-nucleated Microtubules in Assembly and Disassembly Conditions

The analysis described above showed that the microtubules grow continuously above 9.7 μM tubulin concentration. Hence we examined growth in 13 μM tubulin to visualize the ends of growing microtubules.

Fig. 3 shows the ends of microtubules nucleated by a single centrosome on an electron microscope grid in a 13 μM tubulin solution after 3 min of growth in a humidified atmosphere at 37°C (see Materials and Methods for details). Microtubule images are composed of two parallel dark edges surrounding a set of finer dark fringes. One of the edge bands is frequently interrupted close to the end of the microtubule structure which terminates in a long and slightly outward curved extension (Fig. 3, *arrowheads*). The length of these extensions is highly variable between different microtubules and the extremities range from apparently blunt (Fig. 3, *open arrows*) to increasingly long and curved inside-out extensions (*arrowheads*). Occasional top views of tubulin sheets oriented in the plane of the water layer are visible (Fig. 3, *arrows*). Fig. 4 shows details of the range of microtubule end structures observed in assembly conditions. Fig. 4 *a* shows a microtubule end classed as blunt. Fig. 4, panels *b–h* show microtubule ends with one extension of variable length. Fig. 4, panels *i* and *j*

Table II. Catastrophe Frequence at Low Tubulin Concentration

Tubulin concentration	Catastrophe frequency	Percent of time spent in shrinkage	Average velocity	Theoretical steady-state length
	min^{-1}		$\mu m/min^{-1}$	μm
4.5 μM	0.39	3.7	−0.54	1.3
6.5 μM	0.18	3.3	−0.39	4.3

Catastrophic events were observed at the two tubulin concentrations indicated. No rescues were observed in these experiments. The average velocity J of the microtubule population was calculated using $J = \%T_gV_g - \%T_sV_s$, where $\%T_g$ and $\%T_s$ are the percentages of time that microtubules spent respectively in the growing and shrinking phases and V_g and V_s are the average growing and shrinking rates. J was found to be negative indicating that microtubule populations should have reached a steady state length given by $<L> = V_g/f_{cat}$ in the absence of rescues (Verde et al., 1990).

Table III. Variations of the Rates in the Growing and Shrinking Phases

	Tubulin concentration	Mean rate	Standard deviation	Coefficient of variation	Time window	Number of microtubules	Number of rates
	μM	$\mu m/min^{-1}$	$\mu m/min^{-1}$		s		
Growth	4.5	0.50	0.20	0.40	7.6	8	142
	6.5	0.78	0.37	0.48	9.3	10	192
	9.7	1.43	0.58	0.41	9.5	8	132
	13.0	2.18	0.92	0.42	7.6	7	97
	16.2	2.79	1.01	0.36	10.6	6	57
	19.5	3.51	0.90	0.26	13.1	11	110
Shrinkage	4.5	−28.0	5.8	0.21	1.2	7	39
	6.5	−34.9	6.1	0.17	1.9	6	36

Individual rate measurements were performed as indicated in Fig. 1 *b*. The mean rates and their associated standard deviations were calculated from the data given in the histograms of Fig. 2 (*b* and *c*). The coefficient of variation is expressed as the ratio of the standard deviation to the mean rate. The time window corresponds to the average time between two length measurements. The number of microtubules analyzed and the number of rate measurements performed are indicated in the two last columns.

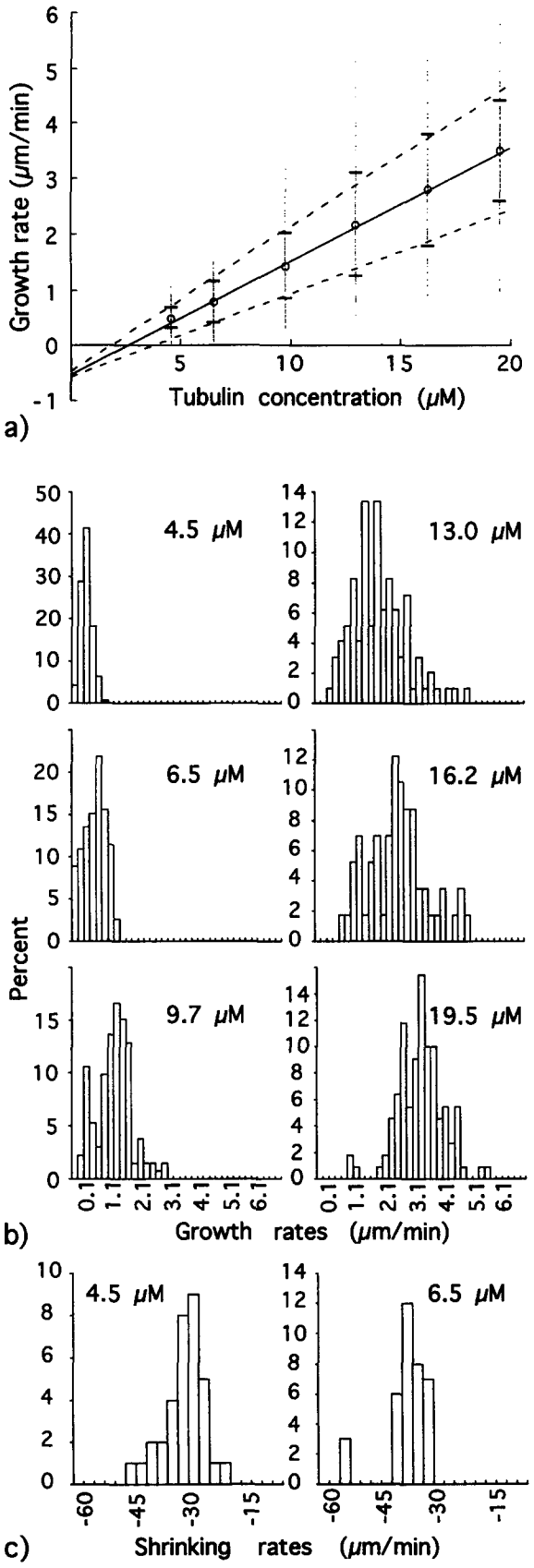

Figure 2. Concentration dependence of the mean growth rate and of the rate variations. (*a*) Growth rate versus tubulin concentration plot. Individual rates (*dots*) measured as in Fig. 1 *b* are plotted at each tubulin concentration. The solid line is a regression through the complete set of data. The growth rate of microtubules is usually described by $V_g = k^+[S] - k^-$. The constant k^+ is the association constant for the GTP-tubulin and is given by the slope of the regression line. Extrapolation of the regression line to the rate axis gives the dissociation constant k^- for the GTP-tubulin and the concentration intercept is defined as the critical concentration for assembly. Rate constants are given in Table I. No assembly was observed at a tubulin concentration of 3.2 μM. The bars indicate the standard deviation associated with the mean rate of each distribution and the dotted lines are regressions through the mean rates plus or minus the standard deviations. (*b*) Histograms of the growth rates at different tubulin concentrations (data were binned every 0.2 μm/min). (*c*) Histograms of the shrinking rates at the two tubulin concentrations where catastrophes occurred (data were binned every 3 μm/min). The mean values of the rates and their associated standard deviations are given in Table III.

show two extensions at the end of a same microtubule and Fig. 4, panels *k–m* show rare views of tubulin sheets. This is representative of the diversity of structures found in a single microtubule aster. However, blunt and one-sided extension ends (Fig. 4, *a–h*) were most frequently observed (see also Fig. 3).

We wished to confirm that the long and curved extensions observed in assembly conditions were not the result of artifactual depolymerization on the grid. Since the video microscope analysis revealed that less than 4% of the microtubule population was disassembling at the lowest tubulin concentrations (Table II), we diluted the specimen on the grid with isothermal buffer to produce large populations of shrinking microtubules. Fig. 5 (*a–d*) shows ends of microtubules polymerized for 3 min at 37°C, diluted 1 to 10 with pre-warmed buffer and incubated for 30 s on the grid before vitrification. These microtubules were clearly shorter after dilution indicating that disassembly had occurred. The end structure of disassembling microtubules were blunt (Fig. 5 *a*), or showed small oligomeric (Fig. 5, *b* and *c*) or coiled structures (Fig. 5 *d*) as previously reported by Mandelkow et al. (1991). The extensions observed under assembly conditions (Fig. 4) were never observed at the end of disassembling microtubules. Fig. 5 (*e–h*) shows examples of microtubule ends classed as depolymerizing but observed under conditions (19.5 μM, 3 min) where no catastrophes occurred. These structures were mainly observed close to the carbon edge suggesting that they have been broken after interaction with it. Therefore, we are quite confident that the sheets observed in growing populations of microtubules reflect the structure of growing ends.

Interpretation of the Cryo-electron Microscope Images

At low resolution (coarser than 30Å for these images), cryo-electron micrographs of thin, unstained specimens correspond to the projection of the electron potential of the specimen on a two-dimensional plane. The microtubule image presented in Fig. 6 shows two large and dense dark edge bands and two finer internal dark fringes. The bottom inset in Fig. 6 is a representation of the relationship between a cross-section of a microtubule and the features seen in projection. The fringes in the center of the pattern correspond to the projection of pairs of protofila-

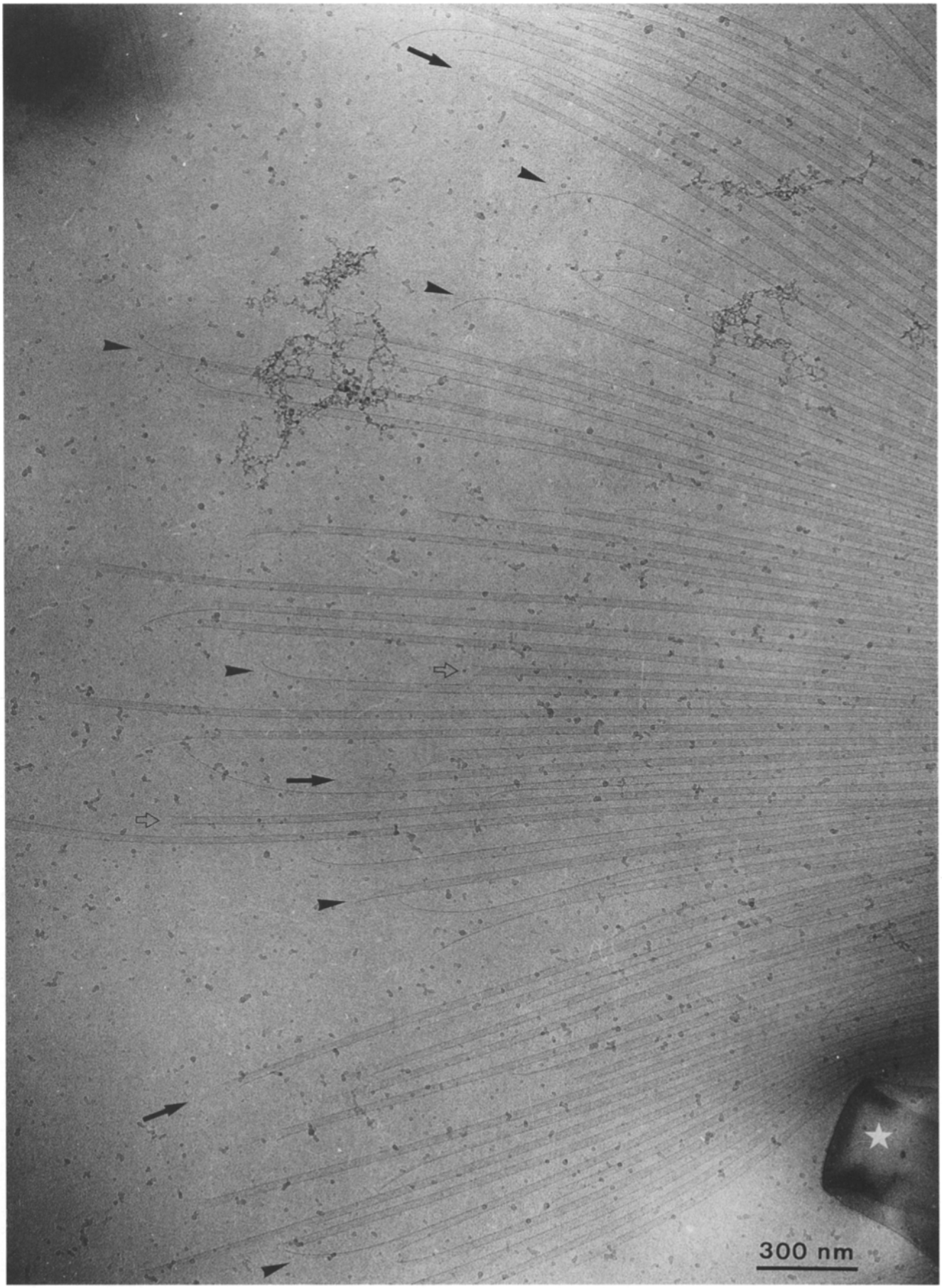

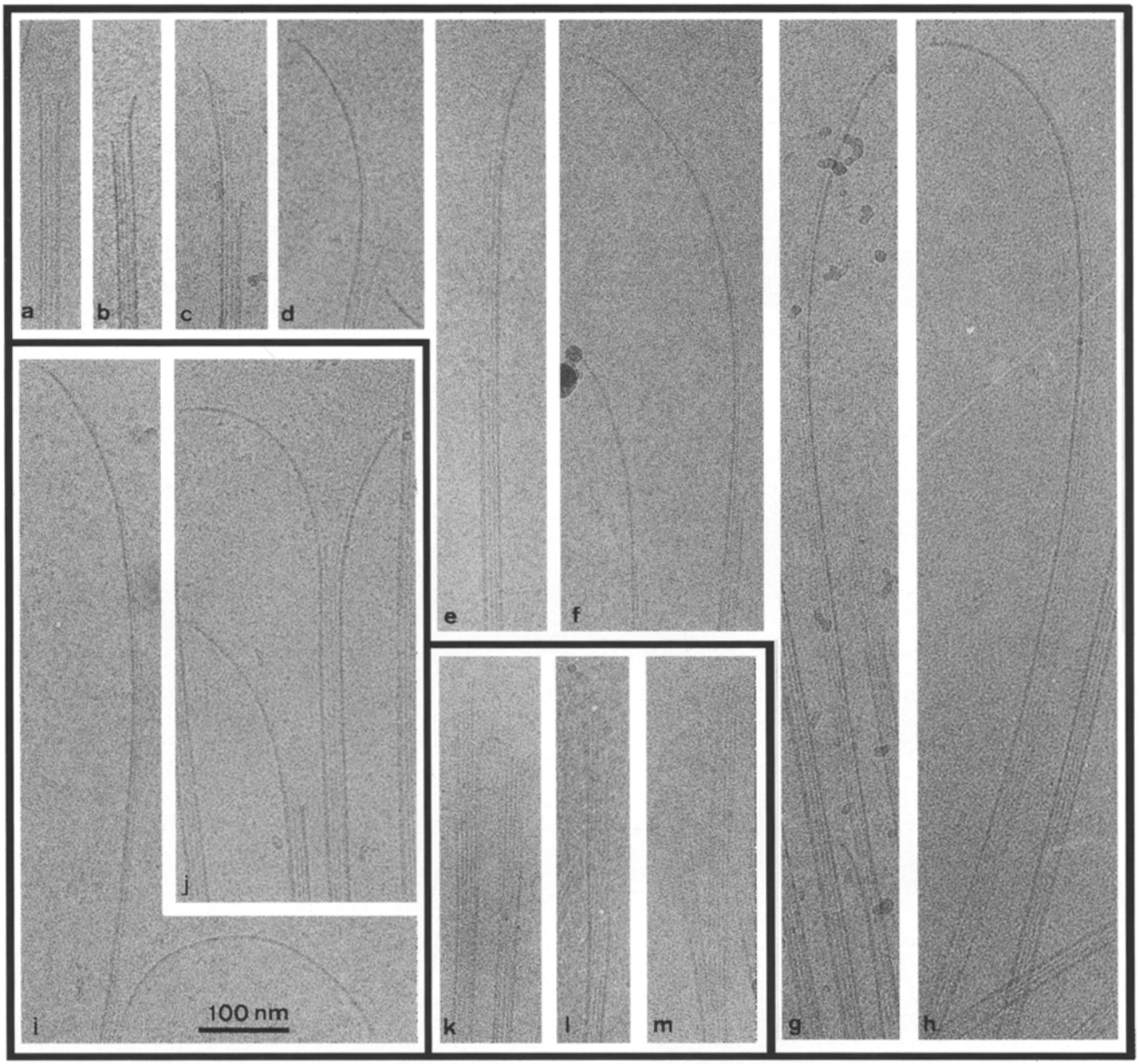

Figure 4. Polymorphism of microtubule ends in assembly conditions. (*a*) Blunt end. (*b–h*) One sided extensions of different lengths. (*i* and *j*) Two sided extensions. (*k–m*) Tubulin sheets.

ments while the dense edge bands delimiting the microtubule image arise from the superposition of several protofilaments (usually 4 to 5). Examination of the extremity at the end of the microtubule in Fig. 6 shows that its contrast is at least as intense as the contrast of the edge bands indicating the presence of several protofilaments in projection (see also Fig. 4 for other examples). The simplest interpretation of this image is that it arises from the superposition of several protofilaments in a plane perpendicular to the image (see top inset), i.e., a curled tubulin sheet (unfortunately, the exact number of protofilaments present in an extension cannot be simply inferred from the image contrast, more structural work will be required to examine this point). The tubulin sheets which are occasionally observed at the ends of growing microtubules (Figs. 3 and 4, panels *k–m*) probably correspond to these extensions. We usually see these sheets oriented side-on because their curvature must be accommodated by the thin water layer. In addition, it is worth noting that the curvature of these extensions tends to increase from the end of

Figure 3. Microtubule aster grown for 3 min at 37°C in a 13 μM tubulin solution and observed in a thin layer of vitrified ice. The extremities are heterogeneous ranging from blunt (*open arrows*) to increasingly long and outward curved extensions (*arrowheads*). Tubulin sheets are infrequently observed (*arrows*). The dark dots are small ice crystals deposited at the surface of the preparation and the large structure at the bottom right of the image (*star*) is a small portion of the carbon substrate.

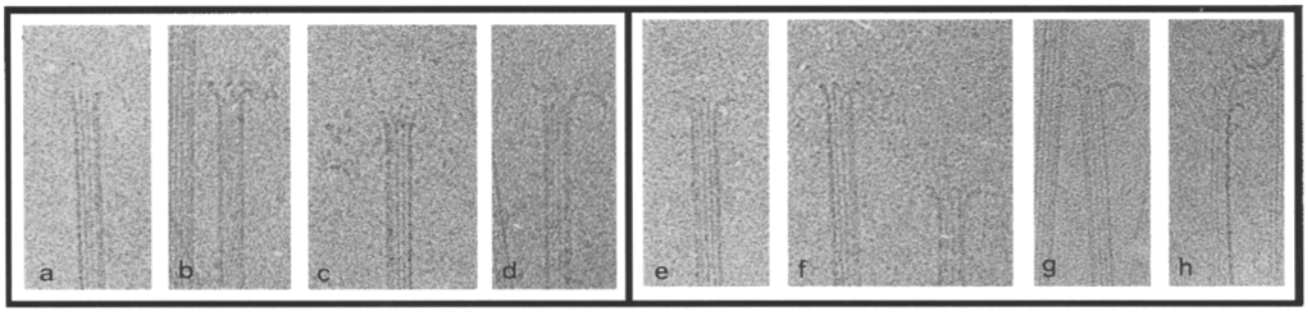

Figure 5. Oligomeric structures present at the ends of shrinking microtubules. (*a–d*) Microtubule ends after isothermal dilution. (*e–h*) Ends typical of depolymerizing microtubules in assembly conditions (19.5 μM, 3 min). The final magnification is identical for all images in Figs. 4 and 5 (bar in Fig. 4 *i*).

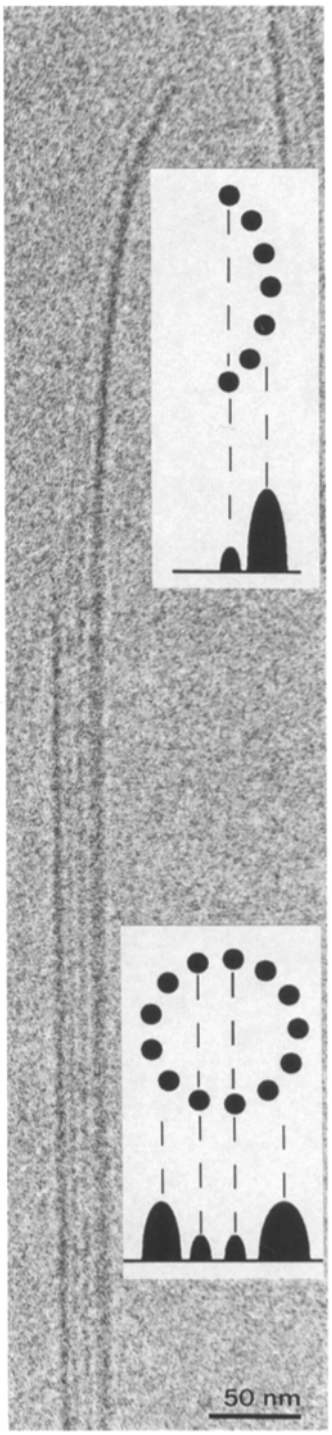

Figure 6. Interpretation of the cryo-electron microscope images. At moderate defocus values (~1.5 μm), microtubule images are characterized by two large and dark edge bands and several finer and less intense internal fringes. The *bottom inset* gives a schematic representation of the image formation in the case of a 13 protofilament microtubule. The two inner dark fringes come from the superposition of two protofilaments in projection and the large edge bands come from the superposition of either 4 (*left*) or 5 (*right*) protofilaments. Note also that due to the odd number of protofilaments the contrast is asymmetric with respect to the longitudinal axis of the microtubule. The contrast present in the image of the extension is at least as intense as the contrast of the edge bands indicating that there must be several protofilaments stacked in this structure (see *top inset*, the number of protofilaments indicated is arbitrary). Note the second finer band running parallel to the intense one which probably corresponds to two protofilaments in projection. This structure would appear flat or slightly "C-shaped" when observed in cross-section.

the microtubule cylinder to the extremity of the extension (see the long extensions in Fig. 4, *e–h*) and that the longer extensions appear more curved than the shorter ones.

Changes in Microtubule End Structure with Assembly Time and Tubulin Concentration

In the previous sections, we have shown that growing and shrinking microtubules have different end structures and that the organization of the subunits in each is distinct from that in the bulk of the microtubule. Growing microtubules display extensions of various length at a given growth rate and these extensions appear to be curled tubulin sheets. We asked whether these structures change with the assembly time and with the average growth rate of microtubules.

Microtubules were grown from centrosomes in the presence of 6.5 μM ($V_g = 0.8 \pm 0.4$ μm/min, $f_{cat} = 0.18$ min^{-1}), 13 μM ($V_g = 2.2 \pm 0.9$ μm/min), and 19.5 μM tubulin ($V_g = 3.5 \pm 0.9$ μm/min) and visualized by cryo-electron microscopy after 0.5 to 5 min of assembly (longer times could not be analyzed because of the increased amount of artifactual breakage of longer microtubules). Fig. 7 *a* shows a microtubule aster after 1 min of assembly in a 6.5 μM tubulin solution. Microtuble ends were blunt or slightly tapered. Fig. 7 *b* shows the extremities of microtubules grown for 3 min at the same tubulin concentration. Longer extensions were observed but a substantial fraction of the microtubules still displayed blunt ends or short extensions. Fig. 7 *c* shows a microtubule aster after 1 min of assembly at 19.5 μM. Comparison with Fig. 7 *a* shows that the number of microtubules nucleated by the centrosome has significantly increased and that microtubule ends displayed longer extensions. Fig. 7 *d* shows the extremities of microtubules grown for 3 min at 19.5 μM. As for the 6.5 μM tubulin concentration, longer extensions were observed at longer times of assembly.

We quantified these changes by digitizing the electron microscope negatives and measuring the length of the extensions at microtubule ends. The results of these measurements are given in the histograms in Fig. 8 and in Table IV. Fig. 8 compares the extension length distributions at the three tubulin concentrations analyzed by cryo-electron microscopy after 1 and 3 min of assembly and between the 6.5 and 13 μM tubulin concentrations after 5 min of assembly. Extension length distributions were inverse exponentials in all cases. The short extensions (<24 nm) represented the main class in most instances (35% at 6.5 μM, 15% at 13 μM, and 8% at 19.5 μM). The mean ex-

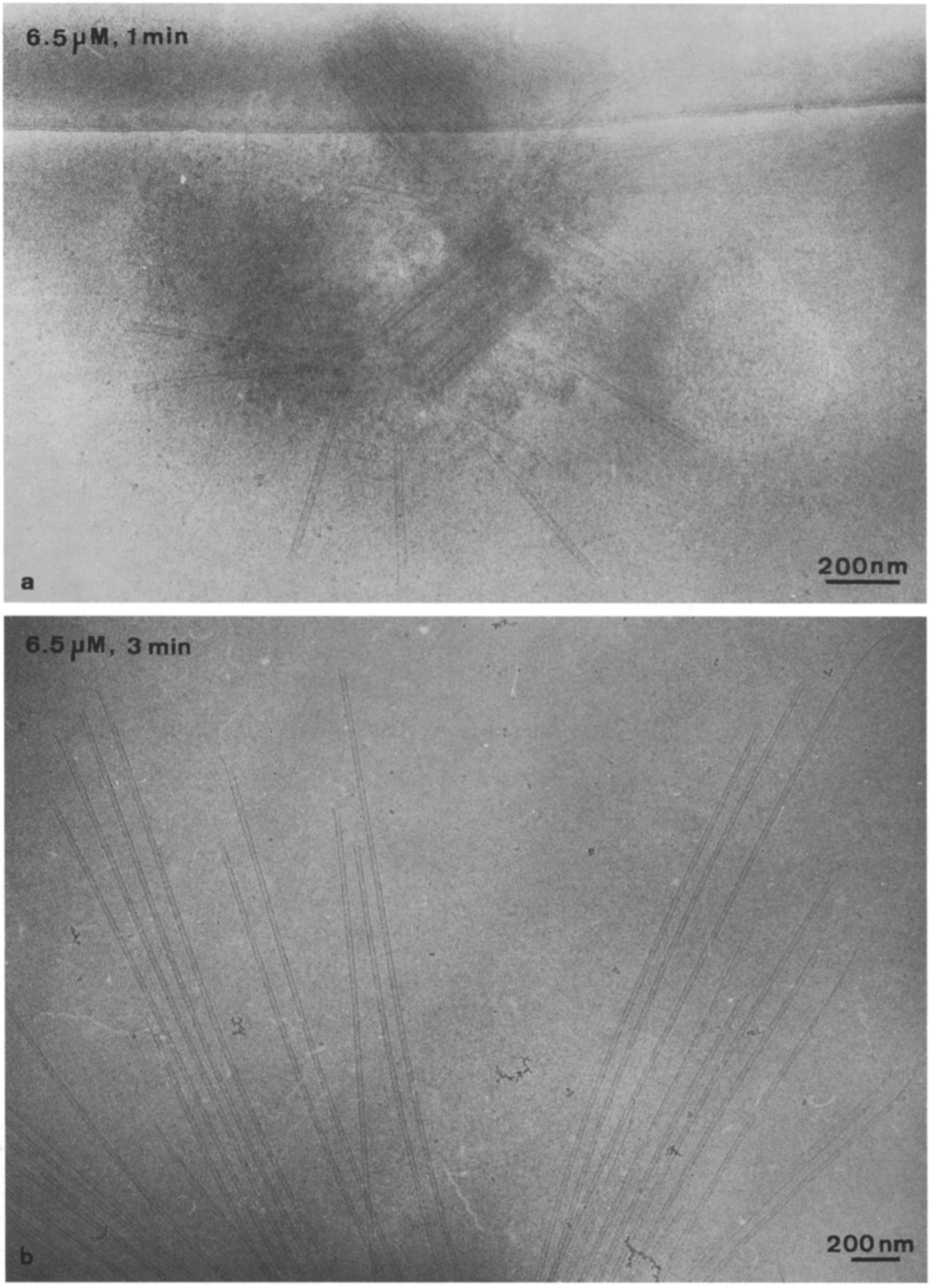

Figure 7. Changes in microtubule end structures with tubulin concentration and assembly time. (*a*) Microtubule aster grown for 1 min in a 6.5 μM tubulin solution. Note that most of the microtubules radiate around one of the two centrioles (see also Fig. 7. *c*). (*b*) Microtubule ends after 3 min of assembly at 6.5 μM. (*c*) Microtubule aster grown for 1 min in a 19.5 μM tubulin solution. (*d*) Microtubule ends after 3 min of assembly at 19.5 μM. Magnification is identical in *b–d*.

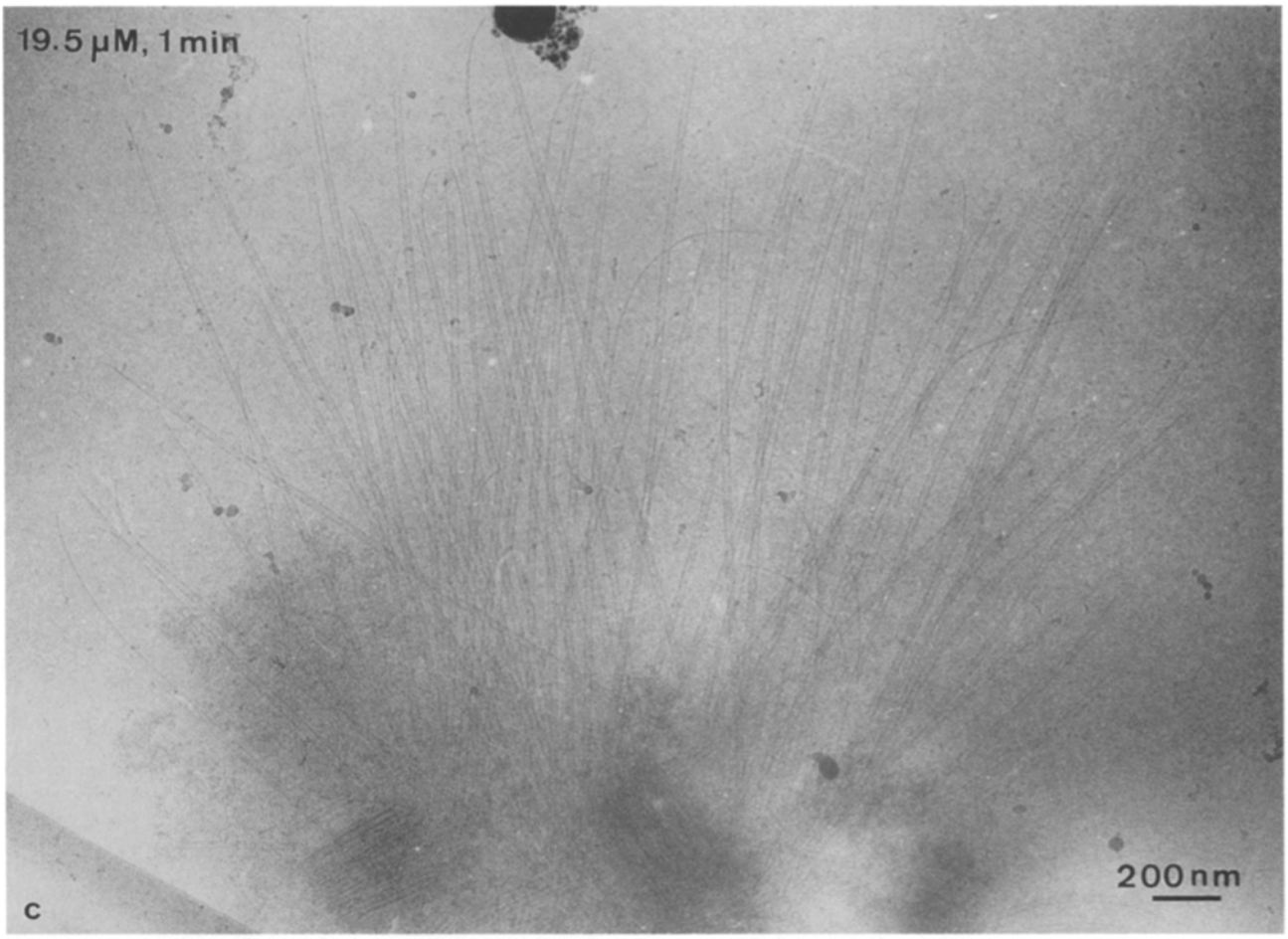

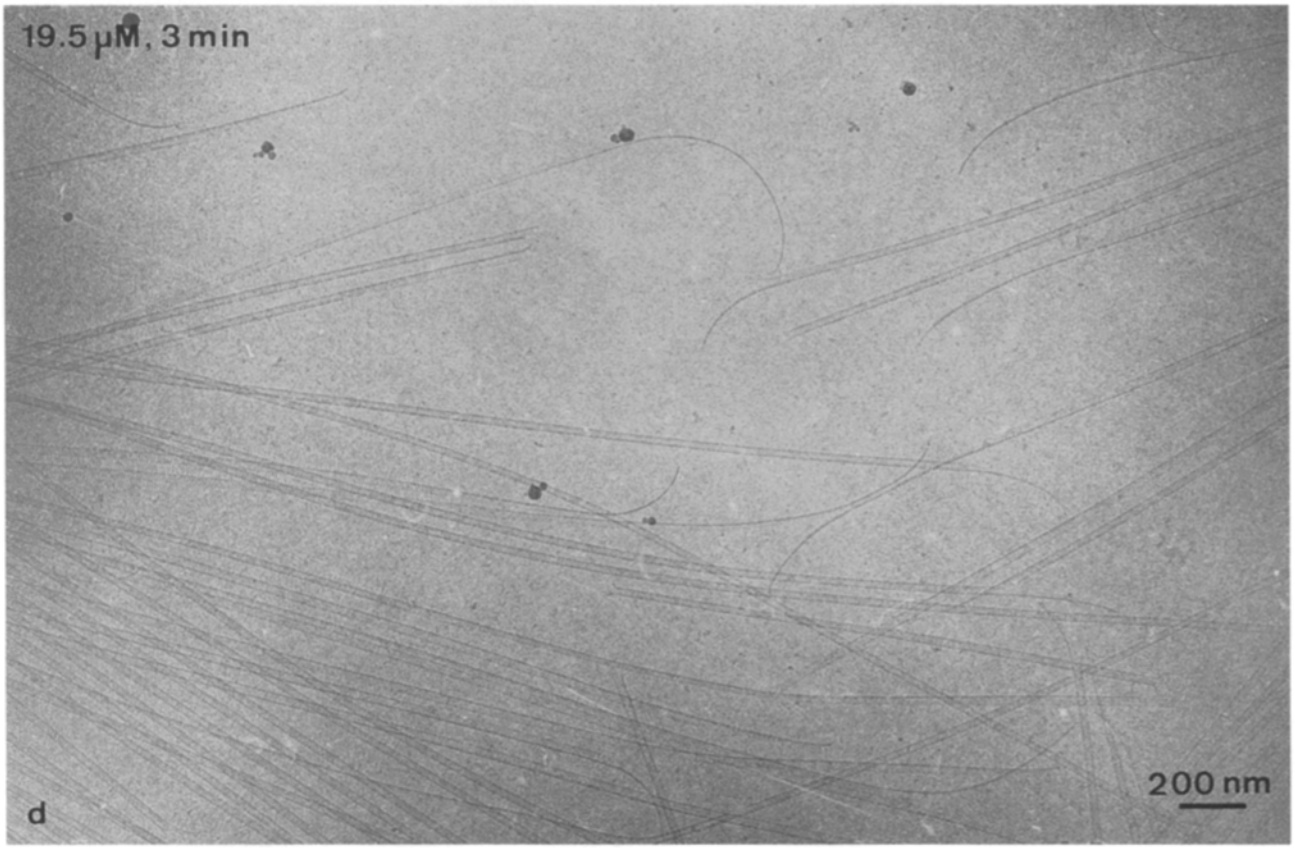

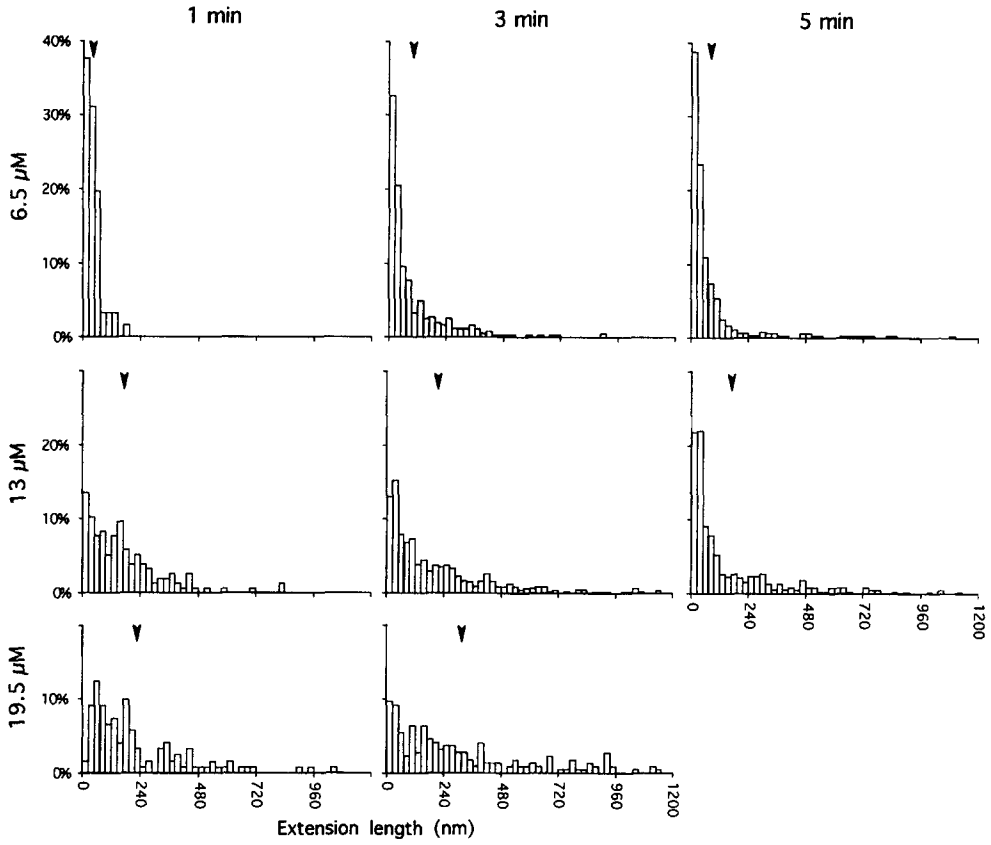

Figure 8. Histograms of microtubule end extension lengths for the 6.5 μM (*top row*), 13 μM (*middle row*) and 19.5 μM (*bottom row*) tubulin concentrations at 1 min (*first column*), 3 min (*second column*), and 5 min of assembly (*third column*). Lengths up to 1.6 μm are plotted in the histograms but extensions as long as 2 μm were measured (see Table IV). The arrowheads indicate the mean of the distributions (data were binned every 24 nm).

tension length (Fig. 8, *arrowheads*) increased with tubulin concentration and time of assembly (see histograms in columns in Fig. 8, see also Table IV). The average lengths of the extensions at 6.5, 13, and 19.5 μM tubulin concentrations were 40, 167, and 227 nm, respectively, after 1 min of assembly, and 98, 209, and 312 nm, respectively, after 3 min of assembly. A comparison of the time evolution of the distributions (compare histograms in rows in Fig. 8) showed that the extension length distributions had a tendency to spread with time and the extent of assembly. The time evolution of the mean of the distributions is shown in Table IV. A clear evolution was observed at 19.5 μM where the mean extension length increased rapidly to 151 nm after 0.5 min and then more slowly to reach 312 nm after 3 min of assembly (see also Fig. 9 *c*, *left column*). The situation was less clear for the two other tubulin concentrations where a decrease in average length occured between 3 and 5 min of growth (Table IV). However, in each case the extensions seen after 3 and 5 min were longer than after 1 min of growth (maximum lengths listed in Table IV). The decrease in mean length after 5 min of incubation is probably a consequence of microtubule disassembly due to artifacts of sample preparation mentioned above. Proper analysis of the distribution of extension lengths at longer assembly times is limited by the occurence of such artifacts.

Table IV. Measurements of Microtubule End Extensions at Different Tubulin Concentrations and Assembly Times

	Mean length	Maximum length	Number of negatives	Number of ends
	nm	*nm*		
6.5 μM				
1 min	40	172	9	61
3 min	98	909	14	365
5 min	80	1093	21	353
13 μM				
1 min	167	834	9	156
3 min	209	1543	24	545
5 min	165	1480	15	386
19.5 μM				
0.5 min	151	653	8	206
1 min	227	1042	5	121
2 min	307	2276	21	499
3 min	312	1924	12	218

Measurements of extension lengths were performed for the three tubulin concentrations at the times indicated in the first column. The mean of the distributions shown in Figs. 8 and 9 *c* (*left histograms*) are indicated. The longest extensions measured are given to indicate the width of the distributions. The number of electron microscope negatives used for each condition and the number of microtubule ends measured are indicated in the two last columns

Modeling of Microtubule Growth

The observation that increasing mean growth rate was correlated with increasing mean extension length suggested that these two phenomena were coupled mechanistically. However, the fact that the extension length distributions had inverse exponential shapes (Fig. 8) and the growth rate distributions had a Gaussian shape (Fig. 2 *b*) indicated that the correlation was not direct. This was also indicated by the fact that the mean extension length continued to change with time while the population was growing at a constant average rate. This meant that one could not predict from the extension length measured at the end of a

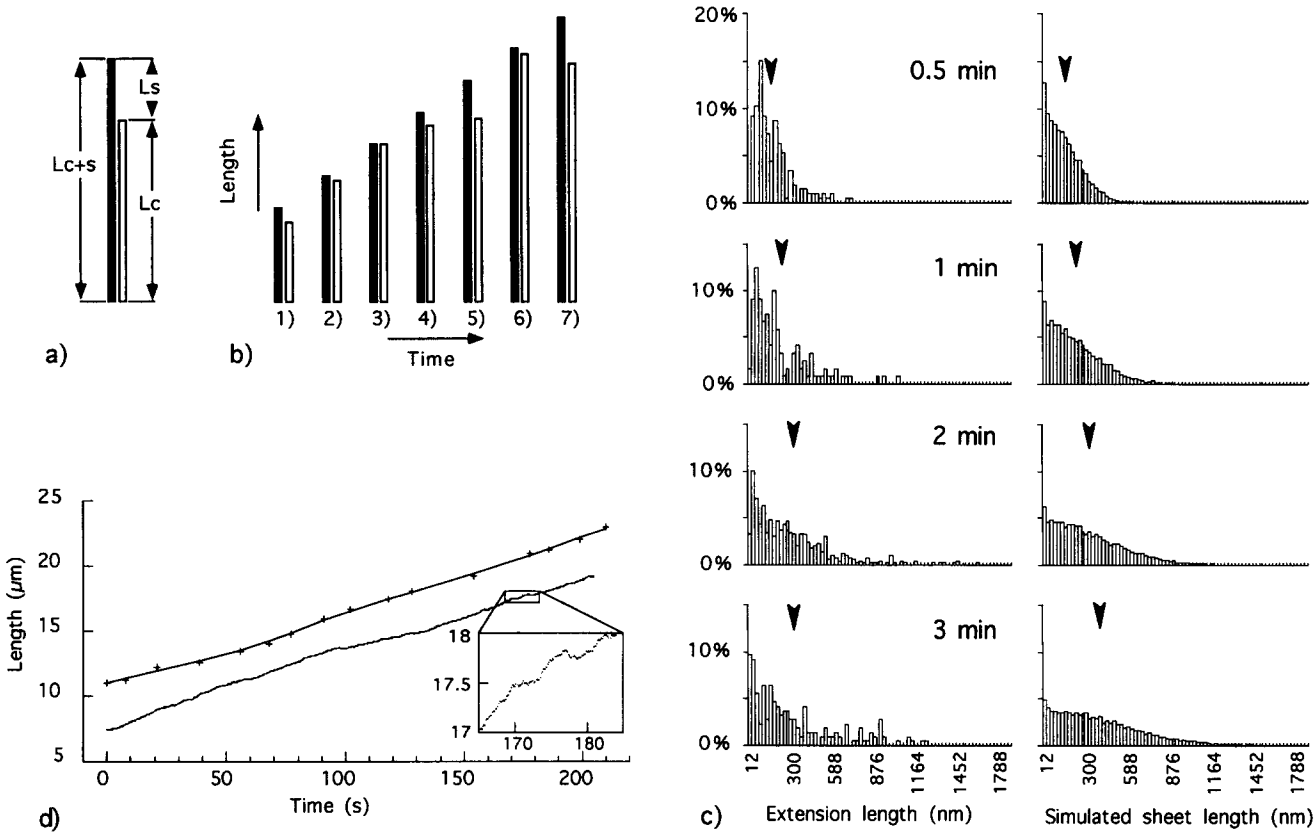

Figure 9. Modeling of microtubule growth. (*a*) Schematic representation of the model. A microtubule is represented by a pair of values corresponding to the length of the complete polymer L_{c+s} (*dark bar*) and to the cylindrical part of the microtubule L_c (*open bar*). The length of the sheet L_s corresponds to the difference between L_{c+s} and L_c. (*b*) Time evolution of the model (see Materials and Methods for details). The complete microtubule structure (*dark bar*) grows at a constant rate by addition of tubulin subunits to its end. The microtubule cylinder (*open bar*) grows at the same average rate but closes and open continuously and cannot be longer than the complete microtubule structure (*step 3*). This model produces "sheets" whose length varies stochastically with time for a single microtubule. Simulation with a high number of microtubules shows that at any time the distribution of sheet length has an inverse exponential shape. The distributions flatten and their mean increase with time (see *c*, *right column*). (*c*) Comparison between experimental extension length (*left*, 19.5 μM) and simulated sheet length distributions (*right*) at different assembly times. The simulation was performed with 10,000 microtubules using a growth rate ($V_g(c) = V_g(s)$ of 3.5 μm/min and a standard deviation of the rate $SD_g(c)$ of 6 μm/min (the time step was 0.137 s). The *arrowheads* indicate the means of the distributions. The standard deviation of 6 μm/min used in the simulation was chosen so that the means of the experimental and simulated distributions were equal at 0.5 min of assembly (data were binned every 24 nm). (*d*) Comparison between an experimental (*top*) and a simulated (*bottom*) L(t) plots at the same average growth rate. (*Top*) Microtubule assembled in a 19.5 μM tubulin solution ($V_g = 3.5 \pm 0.9$ μm/min). Crosses represents experimental points and the line shows the smoothed curve fit through the data. (*Bottom*) $L_c(t)$ plot taken from the simulation shown in *c*. The inset shows an enlarged portion of the simulated $L_c(t)$ plot to demonstrate the small scale variations of length induced by the variations of microtubule cylinder formation rate.

given microtubule whether it was growing rapidly or slowly. This forced us to build a stochastic model using computer simulations based on the experimental information available.

Since most microtubule ends observed by video microscopy were blunt and straight (see Fig. 1 *a*) in contrast to the curved extensions observed by cryo-electron microscopy (Figs. 3, 4, 6, and 7), we assumed that the changes in length observed by video microscopy did not reflect the assembly of tubulin molecules at microtubule ends but rather the formation of the microtubule cylinder from unresolved structures (see Discussion). Our model is also based on the assumption that the extensions observed by cryo-electron microscopy are composed of tubulin sheets which grow at a uniform rate determined by the tubulin concentration. Starting from these considerations we constructed the model illustrated in Fig. 9 (see Materials and Methods for details). The complete microtubule structure, corresponding to the cylindrical part of the microtubule plus the tubulin sheet (Fig. 9 *a*, *dark bar*) grows at a constant rate $V_g(s)$ determined by the tubulin concentration. The value of $V_g(s)$ is given by the video microscope analysis (Table III). The cylindrical part of the microtubule (Fig. 9 *a*, *open bar*) grows at an average rate $V_g(c)$ equal to the sheet rate $V_g(s)$ except that $V_g(c)$ is highly variable. As the distributions in growth rate deduced from the video microscope analysis show Gaussian shapes, we varied $V_g(c)$ with a probability given by a Gaussian distribution of standard deviation $SD_g(c)$. Fig. 9 *b* shows a schematic sequence of the time evolution of the model. Constant sheet growth and variable closure of the microtubule cylinder were simulated independently with the obvious con-

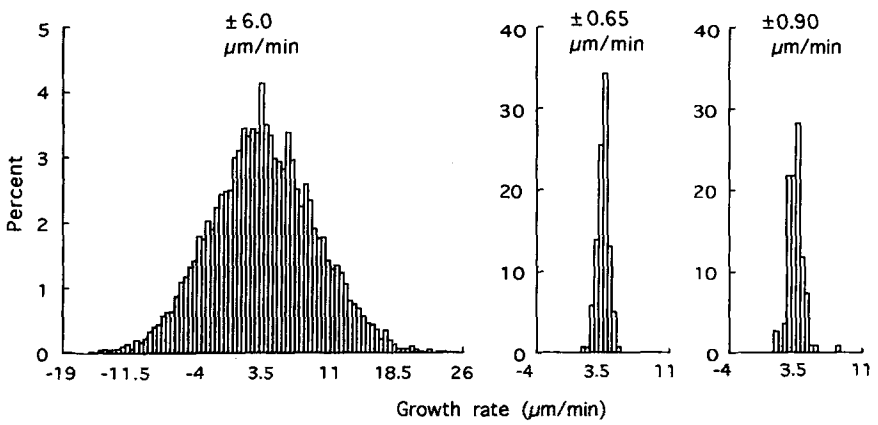

Figure 10. Influence of time averaging of the simulated data on the measured variations of the microtubule cylinder growth rate. The *left histogram* represents the rate variations of a simulated microtubule growing at 3.5 μm/min with an associated standard deviation of 6 μm/min (Fig. 9 *c*). The growth process was simulated with a time step of 0.137 s for 30 min. The *middle histogram* shows the same data averaged every 13 s. This value corresponds to the average time window used between two length measurements in the video microscope analysis of microtubules growing at 3.5 μm/min (19.5 μM tubulin concentration, see Table III). The standard deviation is reduced to 0.65 μm/min. The *right histogram* corresponds to the experimental data at 19.5 μM with an associated standard deviation of the rate of 0.90 μm/min.

straint that the microtubule cylinder could not extend past the tubulin sheet (e.g., Fig. 9 *b*, *step 3*). At the end of the simulation the sheet length L_s was calculated by subtracting the cylindrical part of the microtubule L_c from the complete microtubule structure L_{c+s} for each microtubule (see Fig. 9 *a*) and sheet lengths were binned with the same interval as used for the experimental data.

Fig. 9 *c* compares the experimental extension length distributions at 19.5 μM (*left histograms*) with the simulated sheet length distributions of 10,000 microtubules growing at an identical average rate of 3.5 μm/min (*right histograms*). In order to obtain identical mean values for the experimental and simulated length distributions, it was necessary to increase the experimental standard deviation of the rates to highest values. In the example given in Fig. 9 *c*, the measured standard deviation of the rate of 0.9 μm/min (associated with an average growth rate of 3.5 μm/min, see Table III) was increased to 6 μm/min in order to obtain the same average mean extension and simulated sheet lengths of about 150 nm at 0.5 min. Using this initial condition, we obtained good correspondence between the means of the experimental and simulated distributions at the three other times of assembly (Fig. 9 *c*, *arrowheads*; and see Table V). In addition, the shapes of the distributions were very similar. We compared these distributions by χ^2 analysis and found no significant differences ($P < 0.05$) at the three first times of assembly. However, experimental and simulated distributions were significantly different at 3 min of assembly. Such differences would be explained by the artifacts encountered during the preparation of vitrified microtubules which tend to increase the number of short ends after longer times of assembly. The same comparison was performed for the two other tubulin concentrations used in this study. The standard deviation of the rates used in the simulation ($SD_g(c)$and the mean sheet lengths of the simulated distributions are given in Table V in comparison with the experimental data. Fig. 9 *d* compares a $L_c(t)$ plot of a simulated microtubule (*bottom trace*) taken from the simulation shown in Fig. 9 *c* with an experimental L(t) plot (*top trace*) of a microtubule grown in a 19.5 μM tubulin solution. Although the long range variations in growth rates of the simulated and experimental microtubules are comparable, the simulated trace is much more "noisy" than the experimental one. The box shows an enlargement of the simulated trace indicating that, in our model, the microtubule cylinder does not form at a continuous rate but "closes and opens" stochastically.

To achieve numerical agreement between experimental and simulated data it was necessary to use standard deviations of the rates two- to sixfold higher than those actually measured (see Table V). This reflects the time averaging performed during microtubule length measurements in the video microscope images and in the smoothing of the

Table V. Comparison between Experimental and Simulated Data

Growth rate	Standard deviation			Assembly time	Mean extension length (exp.)	Mean sheet length (sim.)
	Exp.	Sim.	Sim. av.			
μm/min		*μm/min*		*min*	*nm*	*nm*
0.78	0.37	0.7	0.16	1	40	52
				3	98	94
				5	80	124
2.18	0.92	3.6	0.56	1	167	166
				3	209	296
				5	165	384
3.51	0.90	6.0	0.65	0.5	151	153
				1	227	223
				2	307	316
				3	312	391

The first column indicates the average growth rates determined from the video microscope analysis (Table III) for the three tubulin concentrations tested in the cryo-electron microscope experiments and used in the simulations. The standard deviations are indicated for the experimental data (*exp*), the simulated data (*sim*, corresponding to $SD_g(c)$ in the simulation) and the simulated data averaged (*sim. av.*) using a time window corresponding to the one used in the experiments (see Table III, and Fig. 10). The standard deviations indicated in the column (*sim*) have been chosen so that the means of the simulated sheet length distributions equal the means of the experimental extension length distributions for the following time points: 6.5 μM, 3 min; 13 μM, 1 min; 19.5 μM, 0.5 min. The two last columns compare the means of the length distributions determined from the cryo-electron microscope analysis (*exp*) and from the simulations (*sim*) at the different assembly times analyzed.

L(t) plots after curve fitting. Averaging smooths the variation and so reduces the apparent variation in rate in a predictable way. The effect of time averaging can be appreciated by measuring the L(t) histories of simulated microtubules using a time window comparable to that used in the experiment (on the order of 10 s, see Table III). Fig. 10 shows how the standard deviation of the rates is affected by averaging simulated data ($V_g(c) = V_g(s) = 3.5$ μm/min, $SD_g(c) = 6$ μm/min) with a time window of 13 s. The rate distribution determined from the initial simulation is shown on the left histogram. The middle histogram shows the rate distribution after time averaging and the right histogram corresponds to experimental data ($V_g = 3.5 \pm 0.9$ μm/min). The initial standard deviation of 6 μm/min is decreased to 0.65 μm/min after time averaging, a value close to the experimental standard deviation of the rates of 0.90 μm/min measured with an identical average time window of 13 s. The same operation was performed for the other two growth rates using the average time windows used experimentally (given in Table III). In each case the values of the standard deviation of the rates found after time averaging were close to the experimental values (see Table V).

Discussion

Growing Microtubule Ends Are Sheets Which Close to Form Tubes

The results presented here show that the ends of growing microtubules are heterogeneous during assembly, ranging from blunt to long and curved extensions up to several micrometers in length. These structures are clearly different from those observed at the ends of disassembling microtubules which are either blunt or display small oligomeric and coiled structures. Microtubule assembly seems therefore to occur by addition of tubulin subunits to curved sheets that close into a tube.

Sheet formation followed by cylindrical closure has been inferred from earlier work on microtubule assembly (Erickson, 1974; Kirschner et al., 1975) and more recently by Detrich et al. (1985) and Simon and Salmon (1990). Kirschner et al. (1975) used negative staining to analyze the self-assembly of microtubule proteins (tubulin with MAPs) from pig brain. They found long sheets and helical ribbons at the onset of assembly which tend to disappear at the polymerization plateau. Detrich et al. (1985) analyzed the self-assembly of purified sea urchin egg tubulin by turbidimetry and small-angle light scattering and interpreted the overshoot observed before the polymerization plateau as the initial formation of long sheets which later close to form complete microtubules. If we assume that the extensions observed by cryo-electron microscopy and the sheets observed by negative stain electron microscopy correspond to the same structures, our results are consistent with the conclusions of these authors. More recently, Simon and Salmon (1990) used negative staining to observe the end structure of microtubules seeded from axonemes at a tubulin concentration of 14 μM. They found that most of the ends of growing microtubules were blunt but that a significant fraction showed long tubulin sheets up to 6 μm in length. Assembly in the presence of MAPs, which increases the microtubule growth rate and inhibits dynamic instability (Horio and Hotany, 1986; Drechsel et al., 1992), resulted in an increase in the number of sheets. This behavior might be similar to the increase in extension length that we observed at highest growth rate. They also analyzed the end structure of depolymerizing microtubules induced by cold treatment or isothermal dilution and observed mostly blunt ends, whereas we found mainly oligomers after isothermal dilution, in agreement with Mandelkow et al. (1991). Our observations confirm that disassembly occurs via oligomer removal.

The outward curvature of the tubulin sheets observed in our work has not yet been reported by others. This is probably due to their flattening on the carbon substrate when using the negative staining method (Erickson, 1974; Kirschner et al., 1975; Simon and Salmon, 1990). Mandelkow et al. (1991) used a similar cryo-electron microscopic technique to ours and reported that the protrusions were straight, in apparent contradiction with our observations. However the longer protrusions they observed were on the order of 0.2 μm compared with the 2 μm in our study. This might explain why they found that the protrusions were approximately straight (curved protrusions similar to our shortest extensions can also be observed in some of their images, e.g., in Figs. 1 *d* and 7 *a* of their paper). Hence, we think that the straightness of the short protrusions observed by Mandelkow et al. (1991) is not in contradiction with our observations. Short extensions appear straight but as their length increases they tend to curve slightly outward. The curved appearance directly reflects a conformational change in the tubulin molecule during its incorporation into the microtubule lattice. Such a step in microtubule assembly has been proposed by many authors in the past (Kirschner and Mitchison, 1986; Melki et al., 1990; Stewart et al., 1990; Caplow; 1992). Our observations clearly indicate that it occurs.

Variable Growth Rate Reflects the Stochastic Mechanism of Microtubule Closure

Our study provides direct evidence for a difference in end structure between stable and unstable microtubules. Therefore, we tried to design a model of microtubule growth linking the video microscope and the cryo-electron microscope data. In particular this model should reproduce the extension length distributions observed by cryo-electron microscopy and should also account for the large rate variations observed by video microscopy.

Rate variations have been previously observed both during the growing and shrinking phases of dynamic instability (O'Brien et al., 1990; Gildersleeve et al., 1992; Drechsel et al., 1992), but none of the theoretical models elaborated today can account for their presence. The rate variations observed by video microscopy are far too large to be explained only in terms of statistical fluctuations around the equilibrium reaction which sustains tubulin assembly and must reflect some higher molecular process. Changes in protofilament numbers can be ruled out because most of the microtubules nucleated by centrosomes have 13 protofilaments (Evans et al., 1985; personal observations to be reported elsewhere). Other putative causes of rate variability such as isotype diversity have been ruled out by Gildersleeve et al. (1992). These authors proposed

that the most likely origin of rate variations was a fluctuation in the structure of the GTP-cap (Bayley et al., 1990, 1994) or rapid closing and opening of the microtubule cylinder. Our observations and modeling support this later hypothesis. The simple model we propose involves a constant growth of a unique tubulin sheet, followed by its variable closure into the microtubule cylinder (Fig. 9). We tried other models in which more than one extension (up to 13) could grow independently at variable rates. Only models in which the extensions were tightly linked during growth reproduced the experimental extension length distributions. This result is not conclusive since one can always imagine that a more complex model with a greater number of parameters would match the observations. It does indicate that cooperativity between the growth of individual protofilament is present. One important advantage of our model is that it fits all of the available experimental observations without invoking adjustable parameters.

We do not detect curved low contrast extensions at the extremity of most microtubules by video microscopy. Hence we assume in the model that the sheets observed by cryo-electron microscopy are not resolved by video microscopy. This is supported by the following arguments. The contrast of sheets having a protofilament number close to 13 may be lower than that of tubes, leading to a loss of signal in the background subtracted images. In addition, microtubule extremities are subject to rapid movements due to Brownian motion and frame averaging will also lower the signal coming from tubulin sheets. Finally, the practical resolution of the video microscope is about 250 nm (Walker et al., 1988; Salmon et al., 1989). Using a "cut-off" of 250 nm in the extension length distributions presented in Fig. 8 demonstrates that only few extensions should be observed by video microscopy. In fact, occasional curved structures with a lower contrast were observed at the end of growing microtubules (e.g., see the bottom microtubule marked by the white arrow in the top right image in Fig. 1 *a*). They probably correspond to some of the extensions observed by cryo-electron microscopy. Therefore, it seems justified to assume that the growth rate variations observed by video microscopy correspond, for most microtubules, to variations in the closing rate of the microtubule cylinder.

The molecular mechanism that produces the rapid fluctuations between closing and opening states must still be defined. We propose that after addition to the tip of the growing sheet, tubulin subunits undergo a slow conformational change between the tip of the sheet and the beginning of the microtubule cylinder (Fig. 11). This conformational change would accompany the transition from the curved sheet configuration to a straight configuration that precedes closure of the microtubule wall. The closure of the sheet through lateral interactions between adjacent tubulin dimers in the seam region would then depend on the conformational state of the tubulin subunits in this region.

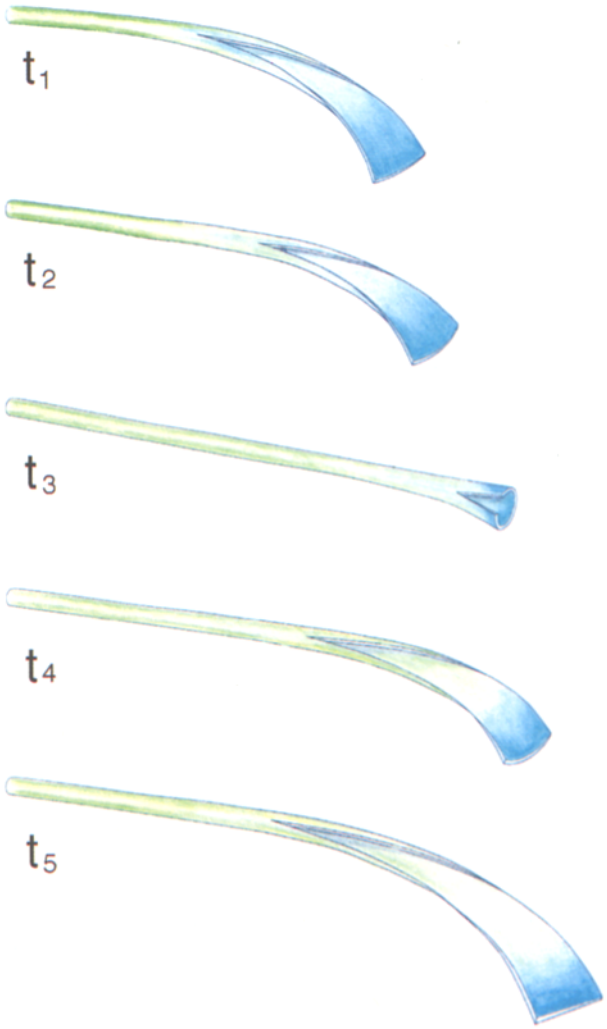

Figure 11. Schematic mechanism of microtubule growth and possible relationship with GTP hydrolysis. Microtubules elongate by formation of an outwardly curved tubulin sheet which closes at a variable rate to form the microtubule cylinder. During this process, tubulin molecules undergo a slow conformational change from the "curved" conformation in the sheet to the "straight" conformation in the cylinder. In addition, the sheet length fluctuates as the result of rapid closing and opening of the cylinder (t_1 to t_5). GTP hydrolysis is supposed to be triggered by this "curve" to "straight" conformational change (t_1) which could produce a gradiant of GTP-tubulins (*blue region*) from the tip of the sheet to the microtubule cylinder (GDP tubulins, *green region*). GTP-hydrolysis also occurs during fast closure of the cylinder (t_2, t_3) which forces the tubulin subunits in the "straight" conformation. Re-opening of the cylinder produces sheets formed of both GDP- and GTP tubulins (t_4, t_5). This mechanism could restrict GTP-tubulins to the terminal subunits at the ends of microtubules.

Microtubule End Structure May Generate Dynamic Instability

The abrupt changes between the slow growing and fast shrinking regimes at low free tubulin concentration must be coupled to GTP hydrolysis (Kirschner and Mitchison, 1986). It was originally proposed that a delay between tubulin assembly and GTP hydrolysis could produce stabilizing "GTP-caps" at the ends of growing microtubules (Mitchison and Kirschner, 1984*a*,*b*). This hypothesis was not supported by measurements of the GTP content in microtubules (O'Brien et al., 1987; Stewart et al., 1990) and dilution experiments (Voter et al., 1991; Walker et al., 1991). These studies showed that GTP-liganded tubulins

must be mainly restricted to the tip of microtubules and that the length of the "GTP-cap" must be independent of microtubule growth rate. Recently Drechsel and Kirschner (1994) have shown that the GTP cap is restricted to the very tip of the microtubule. How can we relate these observations to our model of microtubule elongation? GTP hydrolysis could induce the "curved to straight" conformational change leaving a one-subunit cap layer at the ends of microtubules. However, work with non- or slowly hydrolyzable GTP analogues demonstrate that GTP hydrolysis is not required for microtubule assembly (see Hyman et al., 1992, 1995). This observation suggests that GTP hydrolysis does not induce the conformational change but is rather induced by it. Hence, the conformational change could result from cooperative effects between tubulin subunits in the sheet. According to our model (Fig. 11), GTP hydrolysis would not only follow this gradual conformational change, but could also be forced by the rapid closure of the microtubule cylinder during stochastic alternations between closing and opening states (Fig. 11). Re-opening of the microtubule cylinder would then produce curved tubulin sheets mainly composed of GDP-tubulin molecules. This mechanism implies that short segments of GTP-liganded tubulin would remain at the ends of microtubules and that their length would not have a strong dependence on tubulin concentration and microtubule growth rate. However, due to the stochastic fluctuations in cylinder formation, "GTP-caps" of various lengths should be present at microtubule ends in a given microtubule population. This would explain why different times are observed before fast depolymerization after isothermal dilution near zero tubulin concentration (Walker et al., 1991). At high growth rate, GTP-hydrolysis induced by the rapid closure of the microtubule cylinder would be inhibited by the curved conformation of the terminal subunits in the sheet. At low growth rates, the conformational change occurs at a rate similar to that of cylinder formation, cylinder closure could occasionally reach the extremity of the sheet, forcing GTP hydrolysis in this region and leading to catastrophic microtubule disassembly through a weakening of lateral interactions (Drechsel and Kirschner, 1994).

We are grateful to Brigitte Buendia who helped us with the preparation of centrosomes and tubulin. We also acknowlege Ernst Stelzer and Stephan Albrecht for their development of the video microscope system, and Petra Reidinger for the drawing in Fig. 11. We also thank our colleages Dr. Anthony Hyman (EMBL) and Dr. John Kenney (EMBL) and Dr. Richard Wade (IBS, Grenoble, France) for helpful discussions throughout this work.

This project was supported by European Molecular Biology Organization and Institut National de la Santé et de la Recherche Médicale fellowships to D. Chrétien and HFSP grant (RG. 350/94) to E. Karsenti.

Received for publication 13 May 1994 and in revised form 20 February 1995.

References

Allen, R. D. 1985. New observations on cell architecture and dynamics by video-enhanced contrast optical microscopy. *Annu. Rev. Biophys. Chem.* 14: 265–290.

Bayley, P. M., M. J. Schilstra, and S. R. Martin. 1990. Microtubule dynamic instability: numerical simulation of microtubule transition properties using a lateral cap model. *J. Cell Sci.* 95:33–48.

Bayley, P. M., K. K. Sharma, and S. R. Martin. 1994. Microtubule dynamics in vitro. *In* Microtubules. J. S. Hyams and C. W. Lloyd, editors. Wiley-Liss, Inc., New York. 111–137.

Bornens, M., M. Paintrand, J. Berges, M.-C. Marty, and E. Karsenti. 1987. Structural and chemical characterization of isolated centrosomes. *Cell Motil. & Cytoskeleton.* 8:238–249.

Bradford, M. M. 1976. A rapid and sensitive method for the quantitation of microgram quantities of protein utilizing the principle of protein-dye binding. *Anal. Biochem.* 72:248–254.

Caplow, M. 1992. Microtubule dynamics. *Curr. Opin. Cell Biol.* 4:58–65.

Chambers, M. J., S. C. Cleveland, B. Kleiner, and P. A. Tukey. 1983. Graphical methods for data analysis. P. J. Bickel, W. S. Cleveland and R. M. Dudley, editors. Duxbury Press, Boston. 393 pp.

Chrétien, D., F. Metoz, F. Verde, E. Karsenti, and R. H. Wade. 1992. Lattice defects in microtubules: protofilament numbers vary within individual microtubules. *J. Cell Biol.* 117:1031–1040.

Chrétien, D., and R. H. Wade. 1991. New data on the microtubule surface lattice. *Biol. Cell.* 71:161–174.

Detrich, H. W., M. A. Jordan, L. Wilson, and R. C. Williams. 1985. Mechanism of microtubule assembly. Changes in polymer structure and organization during assembly of sea urchin egg tubulin. *J. Biol. Chem.* 260:9479–9490.

Drechsel, D. N., A. A. Hyman, M. H. Cobb, and M. W. Kirschner. 1992. Modulation of the dynamic instability of tubulin assembly by the microtubule-associated protein Tau. *Mol. Biol. Cell.* 3:1141–1154.

Drechsel, D. N., and M. W. Kirschner. 1994. The minimum GTP cap required to stabilize microtubules. *Curr. Biol.* 4:1053–1061.

Dubochet, J., M. Adrian, J. Lepault, and A. W. McDowall. 1985. Cryo-electron microscopy of vitrified biological specimens. *Trends Biochem. Soc.* 10:143–146.

Erickson, H. P. 1974. Microtubule surface lattice and subunit structure and observations on reassembly *J. Cell Biol.* 60:153–167.

Erickson, H. P., and E. T. O'Brien. 1992. Microtubule dynamic instability and GTP hydrolysis. *Annu. Rev. Biophys. Biomol. Struct.* 21:145–166.

Evans, L., T. J. Mitchison, and M. W. Kirschner. 1985. Influence of the centrosome on the structure of nucleated microtubules. *J. Cell Biol.* 100:1185–1191.

Fumaki, A., and K. Adachi. 1965. A new method of preparation of a self-perforated micro plastic grid and its application. *J. Electron Microsc.* 14:112–118.

Gildersleeve, R. F., A. R. Cross, K. E. Cullen, A. P. Fagen, and R. C. Williams. 1992. Microtubules grow and shorten at intrinsically variable rates. *J. Biol. Chem.* 267:7995–8006.

Horio, T., and H. Hotani. 1986. Visualization of the dynamic instability of individual microtubules by dark-field microscopy. *Nature (Lond.).* 321:605–607.

Hyman, A. A., S. Salser, D. N. Drechsel, N. Unwin, and T. J. Mitchison. 1992. Role of GTP hydrolysis in microtubule dynamics: information from a slowly hydrolyzable analogue Guanylyl-(α,β)-methylene-diphosphonate. *Mol. Biol. Cell.* 3:1155–1167.

Hyman, A. A., D. Chrétien, I. Arnal, and R. H. Wade. 1995. Structural changes accompanying GTP hydrolysis in microtubules: information from a slowly hydrolyzable analogue Guanylyl-(α,β)-methylene-diphosphonate. *J. Cell Biol.* 128:117–125.

Kirschner, M. W., L. S. Honig, and R. C. Williams. 1975. Quantitative electron microscopy of microtubule assembly in vitro. *J. Mol. Biol.* 99:263–276.

Kirschner, M. W., and T. J. Mitchison. 1986. Beyond self-assembly: from microtubules to morphogenesis. *Cell.* 45:329–342.

Krauhs, E., M. Little, T. Kempf, R. Hofer-Warbinek, W. Ade, and H. Ponstingl. 1981. Complete amino acid sequence of β-tubulin from porcine brain. *Proc. Natl. Acad. Sci. USA.* 78:4156–4160.

Maaloum M., D. Chrétien, E. Karsenti, and J. K. H. Hörber. Approaching microtubule structure with the scanning tunnelling microscope. *J. Cell Sci.* 107: 3127–3131.

Mandelkow, E.-M., E. Mandelkow, and R. A. Milligan. 1991. Microtubule dynamics and microtubule caps: a time-resolved cryo-electron microscopy study. *J. Cell Biol.* 114:977–991.

Melki, R., M.-F. Carlier, and D. Pantaloni. 1990. Direct evidence for GTP and GDP-P_i intermediates in microtubule assembly. *Biochemistry.* 29:8921–8932.

Mitchison, T. J., and M. W. Kirschner. 1984*a*. Microtubule assembly nucleated by isolated centrosomes. *Nature (Lond.).* 312:232–237.

Mitchison, T. J., and M. W. Kirschner. 1984*b*. Dynamic instability of microtubule growth. *Nature (Lond.).* 312:237–242.

O'Brien, E. T., W. A. Voter, and H. P. Erickson. 1987. GTP hydrolysis during microtubule assembly. *Biochemistry.* 26:4148–4156.

O'Brien, E. T., E. D. Salmon, R. A. Walker, and H. P. Erickson. 1990. Effects of magnesium on the dynamic instability of individual microtubules. *Biochemistry.* 29:6648–6656.

Ponstingl, H., E. Krauhs, M. Little, and T. Kempf. 1981. Complete amino acid sequence of α-tubulin from porcine brain. *Proc. Natl. Acad. Sci. USA.* 78: 2757–2761.

Press, W. H., S. A. Teukolsky, W. T. Vetterling, and B. P. Flannery. 1992. Numerical recipes in Fortran. Cambridge University Press, Cambridge. 996 pp.

Ray, S., E. Meyhöfer, R. A. Milligan, and J. Howard. 1993. Kinesin follows the microtubule's protofilament axis. *J. Cell Biol.* 121:1083–1093.

Salmon T., R. A. Walker, and N. K. Pryer. 1989. Video-enhanced differential interference contrast light microscopy. *Biotechniques.* 7:624–633.

Simon, J. R., and E. D. Salmon. 1990. The structure of microtubule ends during the elongation and shortening phases of dynamic instability examined by negative-stain electron microscopy. *J. Cell Science.* 96:571–582.

Stewart, R. J., K. W. Farell, and L. Wilson. 1990. Role of GTP hydrolysis in microtubule polymerization: evidence for a coupled hydrolysis mechanism. *Biochemistry.* 29:6489–6498.

Voter, W. A., E. T. O'Brien, and H. P. Erickson. 1991. Dilution-induced disassembly of microtubules: relation to dynamic instability and the GTP cap. *Cell Motil. & Cytoskeleton.* 18:55–62.

Wade, R. H., D. Chrétien, and D. Job. 1990. Characterization of microtubule protofilament numbers. How does the surface lattice accommodate? *J. Mol. Biol.* 212:775–786.

Walker R. A., E. T. O'Brien, N. K. Prier, M. F. Soboeiro, W. A. Voter, H. P. Erickson, and E. D. Salmon. 1988. Dynamic instability of individual microtubules analyzed by video light microscopy: rate constants and transition frequencies. *J. Cell Biol.* 107:1437–1448.

Walker, R. A., N. K. Pryer, and E. D. Salmon. 1991. Dilution of individual microtubules observed in real time in vitro: evidence that cap size is small and independent of elongation rate. *J. Cell Biol.* 114:73–81.

Wordeman, L., and T. J. Mitchison. 1994. *In* Microtubules. J. S. Hyams, and C. W. Lloyd, editors. Wiley-Liss, Inc., New York. 287–301.